Super Resolution Imaging of Protein Aggregates in Cell Models

Tiago Mimoso [a], João Miguel Sanches [a], Tiago Fleming Outeiro [b,c,d]

[a]*Department of Bioengineering, Instituto Superior Técnico, Universidade de Lisboa, Lisbon, Portugal*

[b] *Department of Experimental Neurodegeneration, University Medical Center Göttingen, Göttingen, Germany*

[c]*Max Planck Institute for Natural Sciences, Göttingen, Germany*

[d]*Faculty of Medical Sciences, Translational and Clinical Research Institute, Newcastle University, Newcastle Upon Tyne, United Kingdom*

May 2022

Abstract – Parkinson Disease is one of the most common neurodegenerative diseases in the world. The aggregation of proteins is one possible cause for that which needs to be studied in several aspects such as location and the interactions with the surroundings. The use of confocal and more recent Stimulated emission depletion (STED) microscopy has been one way to understand those mechanisms behind the aggregation. HEK-293T and H4 cells were used to mimic the responses and mechanisms involved. Several protein aggregation models were employed to create a detailed analysis method to use in the images taken from the confocal, STED and expansion microscopy. The method was developed to surpass the lack of the 3rd axis in the analysis, getting the volume of the aggregates and the spatial location of them. Our findings reveal a simple method to have the volume of protein aggregation in the models (Synphilin-1(Sph1) protein tagged with EGFP, fluorescent fragment of GFP - Sph1-GFP aggregation model - and α-Synuclein (αSyn) protein with EGFP truncated with just 83 amino acids) and Sph1 protein tagged with V5 - SynTWT+Sph1 aggregation model-). The findings reveal that there are some differences regarding the microscopy technique used in terms of volume and the number of aggregates per cell. In the SynTWT+Sph1 aggregation model, the colocalization between the proteins seems to be out of phase on the Z axis. This method allows us to be more time effective and less biased to the user since the data to train the model can be universal or have more manual analysis from several users which diminish the human error.

Keywords: α-Synuclein, Synphilin-1, Super-Resolution Microscopy, Segmentation, Deep Learning, Volume

Introduction

Parkinson's disease (PD) affects around 1%-1.5% of the total population (Vidyadhara et al., 2019). With the increase of the average age among the population, these age-dependent disorders are becoming a threat to human health and (Gitler et al., 2017) could achieve astonishing numbers by 2050. The main protein linked to PD is αSyn (Goedert, 2001). The correlation between αSyn aggregation and conformational changes and PD have been studied for the past 20 years, describing this protein as having the central role in the development and progression of the disease (Marvian et al., 2019). After gene sequencing of PD patients, some mutations in the gene encoding α-Synuclein (SNCA) have been found and some of those mutations were linked to the dominantly inherited forms of PD, the familiar form of PD, which only represents 5% (Bossy-Wetzel et al., 2004). The dogma that is still being discovered is how sporadic PD occurs, which represents around 95% of the disease cases (Valente et al., 2012).

Therefore, the development of PD involves several factors. Studies suggest that polymorphisms in the genes that are responsible for dopamine metabolism and transport, iron homeostasis, inflammation, mitochondrial dysfunction and exogenous or endogenous toxin metabolism might play a role in individual predisposition to developing PD (Huang et al., 2004). Affecting the presynaptic αSyn, these proteins create micro aggregation which theme impaired neurotransmitter release leading to postsynaptic degeneration (Schulz-Schaeffer, 2015). Also, in its aggregation, it is created LB which is a way to classify PD.

αSyn took a central stage in the research in recent years and now presents a central role to achieve the knowledge of the disease (Outeiro & Mestre, 2019). *In vitro* studies using recombinant αSyn were instrumental to inform about the aggregation process that culminates with the formation of typical amyloid fibrils (Conway et al., 2000; Li et al., 2001). *In vivo* studies in human αSyn transgenic and in knockout mice provided insight into both its physiological function and into the mechanisms of toxicity (Burré et al., 2010; Greten-Harrison et al., 2010). *In vitro* studies, using mammalian and yeast cell models, yielded important insight into the molecular underpinnings of αSyn aggregation, cytotoxicity, and physiological effects (Lázaro et al., 2014; McLean et al., 2000), and into the pathways involved in the production and clearance of the protein in the cell. The explosion in the field of proteostasis in the 2000s, brought about an important knowledge on how cells and organisms handle αSyn, attempting to refold or recycle the protein into its basic components (Cuervo et al., 2004).

More recently, technological developments in biochemical, biophysical, proteomic, and imaging approaches, provided insight into the structure, chemical modifications (posttranslational modifications, PTMs), and subcellular distribution of αSyn (Gonçalves & Outeiro, 2013).

The formation of aggregation found in Parkinson's disease is not only composed of αSyn, some of them also composed by Sph1 (Shirakashi et al., 2006). Sph1 is also a presynaptic with synaptic

vesicles (Ribeiro et al., 2002) also present in LBs as well as αSyn, especially in the core region (Wakabayashi et al., 2001). Co-expression of αSyn and Sph1 in cellular models gives rise to eosinophilic cytoplasmic inclusions, and the overexpression of Sph1 alone can also produce inclusions in cultured cells. Additionally, Sph1 overexpression increases the vulnerability to the toxicity of proteasome inhibitors (Tanaka et al., 2004).

Recent studies show that synphilin-1 contains four ankyrin repeat domains and a coiled-coil domain in the central portion that specifically interacts/binds with αSyn, via the N-terminal residues of αSyn (Xie et al., 2010). This specific interaction significantly promotes formation and accumulation of cellular inclusions that are probably composed of αSyn (Xie et al., 2010).

Microscopy has been one of the best sources of information in several areas like biomedical science or even materials science. Developing these techniques is mandatory to assist different areas of interest. The overcoming of the diffraction limit, the possibility of removing the out-of-focus light from the detector are some of the achievements that have been already done before, however, more challenges are existing to overcome for the field.

The confocal microscopy increases the resolution compared with conventional optical microscopy due to the fact of having the Pinhole which leads to the exclusion of the light from the non-focal plane. To explain it in a better way. Using the conventional microscope the record in the focal plane will be the fluorescence of all samples instead, in the confocal microscopy, using the pinhole of the epifluorescence microscopy which is able to deny the fluorescence from the non-focal plane (Pawley, 2006).

The STED microscopy is based on the confocal where it excites the sample with fluorescence particles and then a second laser bean where it is depleted of some of those fluorescence. Using this technique, the Abbe diffraction limit is overcome, and the wavelength barrier is broken. The excitation and STED beans are triggered at different times to get the better resolution. The resolution of the STED microscope is a function of the spatial distribution and magnitude of the intensity of the depleting light, with no theoretical limit to the ultimate achievable value. Nonetheless, the nature and factual quality of the focal intensity patterns of the STED beam strongly impacts the resolution achieved by a particular configuration. Typically, a doughnut shaped distribution is targeted to obtain the most uniform resolution increase in the focal plane.

Expansion microscopy (ExM) is a novel super-resolution microscopy technique that was developed with the intent of creating a technique that was not bound by the necessity of very expensive microscopy. The ability of using in any setup becomes of the most advantage of this method as all the effects are done on the sample (Truckenbrodt et al., 2018). ExM, a technique introduced by the Boyden laboratory, is an important step in the direction of becoming the biological samples that had enough resolution without special equipment (Chozinski et al., 2016).

However, there are several techniques that allow us to image those protein aggregates, the question of which one should we apply still be unsolved. Therefore, using several techniques in those aggregation model to mimic the effects of the PD could lead to several discoveries. The work presented in this thesis aims to develop one method to analyze the volume of the aggregates. After the volume analysis, the colocalization between the Sph1 and SynTWT protein are analyzed as well. Comparing the differences between confocal and STED microscopy is another goal for this study.

Materials and methods

Preparation and acquisition of biological data

The collection of the biological data can be divided into four main stages: Cell culture, cell transfection, immunocytochemistry, and imaging. Each of these sections will be described in detail in the sections below.

Cell culture

There were two types of cells to study the aggregation models. Kidney epithelial cells (HEK) were used to study the aggregation of Sph1-GFP while Human neuroglioma cells(H4) were used to study the SynT WT with Sph1 aggregation model. HEK cells are cultured in DMEM medium®(Life Technologies) supplemented with 10% Fetal Bovine Serum and 1% Penicillin /Streptomycin. The cells were grown at 37◦C in an atmosphere of 5%CO2. Human neuroglioma cells (H4) were maintained in OPTI-MEM®(Life Technologies) supplemented with 10% Fetal Bovine Serum and 1% Penicillin/Streptomycin. The cells were grown at 37◦C in an atmosphere of 5%CO2.

Metafectene Transfection

This method of transfection was used exclusively in HEK cells. 1µg of DNA and 50µL of OPTIMEM® (Life Technologies) have been mixed. Meanwhile, in another Eppendorf, 2µg of Metafectene and 50µL of OPTIMEM have been mixed. After 5 minutes, both solutions are mixed and left to rest for 20min (Biontex, n.d.) Finally, 100µL of the solution is mixed in a 12 well-plate for at least 24h. 24h later, the medium of the cells is changed to the cell culture medium. After 48h, the transfection is stopped by fixation with 4% paraformaldehyde (PFA).

Fugene Transfection

This method was used for the H4 cells. As described by the manufacturer, 100uL of OPTIMEM®(Life Technologies) and 6uL of Fugene (Promega). After 5 min,1ug of DNA (SynT WT and Sph1) was added and left to rest for 30min and, finally, 100µL of the solution was mixed in a 12 well-plate for 48h.

Immunocytochemistry

After the transfection and the fixation of the cells with PFA 4%, were washed three times with PBS1x around 5min in the shaker. Then, it is incubated with Tritton-1x in PBS, shaking.

After 10min, a blocking solution (3% BSA in PBS 1x) was added and left it at Room Temperature (RT) on the shaker. In that hour, the solution with the first antibody is prepared where depending on the type of microscopy used the concentration can change (1:1000 in Confocal and STED Microscopy and 1:100 in Expansion Microscopy), the solution is prepared in the blocking solution previously prepared. After the incubation overnight of the primary antibody, the cells

are washed with PBS1X three times around 5 min each wash. In Sph1 aggregation model, it was used the fact of having the tagged GFP as way of collecting the signal. In SynTWT+Sph1 aggregation model, 1:1000 Anti-SynTWT Mouse and 1:1000 Anti-SphV5 Rabbit were used as primary antibodies and 1:1000 Anti Mouse Alexa 488 and 1:1000 Anti Rabbit Alexa 555 were used as secondary antibodies in confocal microscopy. 1:1000 Anti-SynTWT Mouse, 1:1000 Anti-SphV5 Rabbit and 1:1000 Anti-Tubulin Rat were used as primary antibodies and 1:1000 Anti Mouse STAR635P, 1:1000 Anti Rabbit Alexa 594 and 1:1000 Anti Rat Alexa 488 as secondary antibodies in STED microscopy.

Meanwhile, the secondary antibody solution is prepared with the blocking solution with different concentrations of antibody (1:1000 in Confocal and STED microscopy and 1:100 in Expansion Microscopy). The cells were incubated for 1h at RT on the shaker and then, the cells were washed again with PBS 1x three times around 5min each wash.

As the nucleus is one region of interest, after the final step, the DAPI solution (1:1000) was added for 5 min and then washed again with PBS1x. Mowiol is used to mount the slides and, finally, the slides are left to dry at RT covered from the light.

In Sph1 aggregation model, tagged GFP was used to collect the signal because of the inherent effect of fluorescent. In SynTWT+Sph1 aggregation model, 1:1000 Anti αSyn Mouse (BD, USA) and 1:1000 Anti V5 Rabbit (Abcam, UK) were used as primary antibodies and 1:1000 Alexa Fluor 488 donkey anti-mouse IgG (Thermo Fisher Scientific, USA) and 1:1000 Alexa Flour 555 goat anti-rabbit IgG (Invitrogan, USA) were used as secondary antibodies in confocal microscopy. 1:1000 Anti-SynTWT Mouse, 1:1000 Anti-SphV5 Rabbit were used as primary antibodies and 1:1000 Alexa Fluor 594 goat anti-rabbit IgG (Thermo Fisher Scientific, USA), 1:1000 Abberior Star 635P goat anti-mouse IgG (Abberior, Germany), 1:1000 Alexa Fluor 488 donkey anti-rat IgG (Thermo Fisher Scientific, USA) as secondary antibodies in STED microscopy

Confocal Microscopy

Imaging was conducted on a ZEISS LSM 800 using 100X and 1NA objective. Each collected image represents a range of z-slides (32 slices in Sph1-GFP and 24 slices in SynTWT+Sph1aggregation model) with the information of the entire cell. The dimensions of each image are 2048x2048 px (30,1 nm in Sph1-GFP aggregation model and 41,2 nm in SynTWT+Sph1 aggregation model).

Each aggregation model was was imaged in different experimental groups. There are 3 experimental groups to consider for the Sph1-GFP aggregation model: Negative Control, Positive Control and Experimental groups.

There are 7 experimental groups for SynTWT+Sph1 aggregation model: Negative control, Positive control, Group 1 with just primary antibody and group 2 with only secondary antibody, SynTWT (group 3) and another group to evaluate the Sph1 (group 4) and the experimental groups.

STED microscopy

The imaging of each model was conducted in a different setup due to physical limitations of the lasers and the goal of resolution in z axis.

Imaging the Sph1-GFP aggregation model was conducted on a Custom setup described in (Willig et al., 2014) using 100X and 1NA objective. This setup was based on (Wegner et al., 2017). The dimensions of each image are different for each cell (20nm/px). Each image collected represents a range of z-slides (200 nm/px) to have information of the entire cell.

Imaging the SynTWT+Sph1 aggregation model was conducted on a Custom setup (van Dort, 2018; Wegner et al., 2017) using 100X and 1.4 NA objective (HCX PL APO 100x/1.40 OIL STED, Leica Microsystems, Wetzlar, Germany). Each image collected represents a range of z-slides (100nm/px) to have information of the entire cell. The dimensions of each image are different for each cell (40nm/px). This model had the advantage of using a 3D STED which helps in the resolution in the z direction.

Expansion Microscopy

The expansion protocol was performed as described in (Truckenbrodt et al., 2019). After immunocytochemistry, the samples were incubated overnight with 500µl of Anchoring buffer (1x PBS + 0.1mg/ml Acryloyl-X (Life Technologies, Carlsbad, CA, USA)) at RT.

The day after, the samples were washed with 1x PBS three times for 5 min, and the polymerization solution was applied. For the X10 gelling solution, 33% (w/w) of high purity sodium acrylate (SA) and N,N-dimethylacrylamide acid (DMAA) monomers solution was dissolved at a molar ratio of 4:1 (DMAA:SA) in ddH2O. The polymerization solution was bubbled with nitrogen gas for 40 min at RT. In a separated tube, potassium persulfate (KPS) (0.036 g/ml stock of KPS) was prepared at 0.4 molar% relative to the monomer concentration and mixed with the DMAA+SA solution. Another 20 min of bubbling with nitrogen gas was performed in a mix of ice + water to keep the temperature homogeneous and closer to 0ºC as possible. For 1ml of gelling solution, 4µl of N,N,N′,N′-tetramethyl-ethane-1,2-diamine (TEMED) was added. Then, 60µl of the solution was applied into the chamber prepared previously according to (Truckenbrodt et al., 2019). The polymerization took between 1-3 days, after that period. Then, the gel from the polymerization was incubated overnight in a humid chamber with digestion buffer (50mM of TRIS + 800 mM guanidine HCL + 1mM EDTA + 0.5% (vol/vol) Triton X-100) and Proteinase K in a concentration of 1:100.

Imaging was performed on a Zeiss Axio Observer (ZEISS, Germany) with an Air 20X objective and 0.25 NA. The estimation of the Expansion Factor was done using the expression (Equation 1), which was calculated using 50 nuclei of pre-expansion cells and 50 nuclei of post-expansion cells.

$$Expansion\ Factor = \frac{\sqrt{\sum Area_{Post}}}{\sqrt{\sum Area_{Pre}}} \quad (1)$$

Digital Processing

The Processing of the data can be divided in four steps: 3D matrix creation of each channel of interest; the 2D segmentation using the Stardist Network (Schmidt et al., 2018; Weigert et al., 2020)the relationship between the segmented areas and finally

the statistical analysis.

Deep Learning Algorithm

Model training was performed by recurring to pictures given by Liana Shvachiy of the same aggregation model used in the experimental data (150 for SynTWT+Sph1 aggregation model and 87 pictures to Sph1-GFP aggregation model). The channel of interest needs to be taken in consideration due to heterogeneity between the channels, in other words, for every channel a model must be created in separate. Then, the model was used to segment in 2D.

Creation of the mask

To have one cell per image, the pre-analysis was performed to create masks for each picture to make sure that just one cell was taken in consideration.

Relation of segmentation

The 2D segmentation of each layer was related though masks with a previous list of objects already taken as possible aggregates. Then, the fact that each aggregate needed to be convex and continuous in the z axis was taken into consideration. In each layer, there are3 possibilities: the segmented area can intersect with just one possible aggregate; the segmented area can be alone and no interaction with any possible aggregates; or the segmented area can interact with more than one aggregate. In the first two options, the solution looks obvious, when there is an interception, a new possible aggregate is added to the list, when there is just one intersected aggregate, then the volume of that layer is added to that object with the replacement of the new mask. When there is more than one possible aggregate, the volume of all possible aggregates is added, and it is by replacing those possible aggregates by one with the merge of those aggregates. In the end of the process, the possible aggregate with just one layer was removed because of the low probability of having so small aggregates.

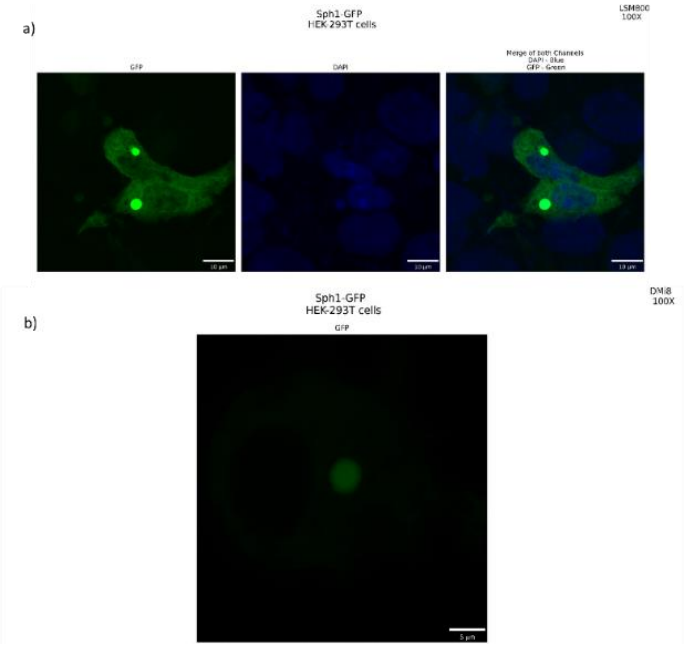

Figure 1 . Representative MIP images from the SphGFP model. a) MIP taken in consideration as a standard image from confocal microscopy. Images taken at 100x magnification. Scale bar 10µm. b) MIP to taken in consideration as a standard image from STED microscopy. Images taken at 100x Scale bar 5µm.

Colocalization

In the SynTWT+Sph1 aggregation model, an object-based colocalization was performed where it was analysed the intersection of the Sph1 over the SynTWT signal. This value was removed in each layer using the predicted from the model. Then, for each image (and cell) the average colocalization and the maximum was taken as results.

Statistical Analysis

Volume of Aggregates was calculated per experiment and standard deviation of each batch. and Standard Deviation of Volume of Aggregates per Cell and the number of aggregates per cell were analyzed. Regarding the colocalization, the average and standard deviation was done as well.

Results

Design the Maximum Intensity Projection in both aggregation models

To evaluate the aspect of the image to ensure that the analysis is performed in a cell with aggregates, the maximum intensity projection (MIP) was created in each aggregation model and type of microscopy. Imaging from confocal and STED microscopy was done, obtaining representative MIP images from each aggregation model and type of microscopy (Figure 1 and Figure 2). Regarding the Sph1 GFP aggregation model it was expected to get lower number of aggregates comparing with the other aggregation model although with large volume comparatively with the size of the cell. Though the MIP, it is possible to observe the results expected without any quantification. This observation is merely qualitative. (Figure 1 and Figure 2)

To evaluate the same goal in the other model (SynTWT+Sph1 aggregation model), it was created MIP (Figure 2) where it is possible to detect a lot or aggregates in both channels (αSyn and Sph1). The size of the aggregate can vary with some of them being relatively medium size while the most of them are small in area.

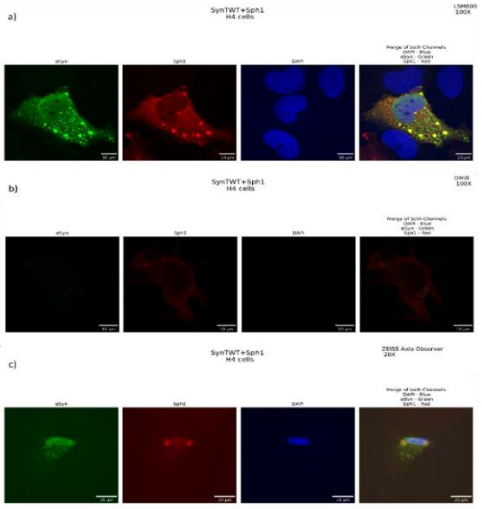

Figure 2. Representative MIP images from SynTWT+Sph1 aggregation model. a) MIP taken in consideration as a standard image from confocal microscopy. Images taken at 100x magnification. Scale bar 10µm b) MIP taken in consideration as a standard image from STED microscopy. Images taken at 100x magnification. Scale bar 10µm c) MIP taken in consideration as a standard image from ExM images taken at 20x magnification. Scale bar 20µm.

Localization and quantification of the aggregates

Table 1. . Values of average and standard deviation regarding the volume of aggregates, number of aggregates per cell and the average volume of aggregate per cell in Sph1-GFP aggregation model.

Type of Microscopy	Average Volume of aggregates [µm³]	Average Number of aggregates per cell [aggregates]	Average Volume of aggregates per cell [µm³]
Confocal Microscopy	32,36 ± 62,59	3 ± 2	50,75 ± 55,77
STED Microcopy	6,44 ± 27,39	8 ± 13	24,57 ± 37,60

To access the position of the aggregates together with its volume, several statistical metrics was evaluated (volume of aggregates, number of aggregates per cell and volume of aggregates per cell). This metrics were applied in both microscopies as well as in both aggregation model.

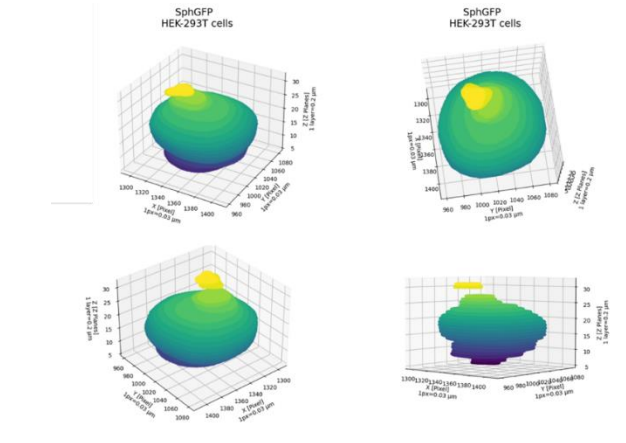

Figure 3. Several views of the 3D projection from confocal microscopy in the Sph1-GFP aggregation model. These views are the analysis of the segmented areas and MIP image from confocal microscopy and Sph1-GFP aggregation model.

In Sph1-GFP aggregation model, as it was expected that the results provide differences in terms of

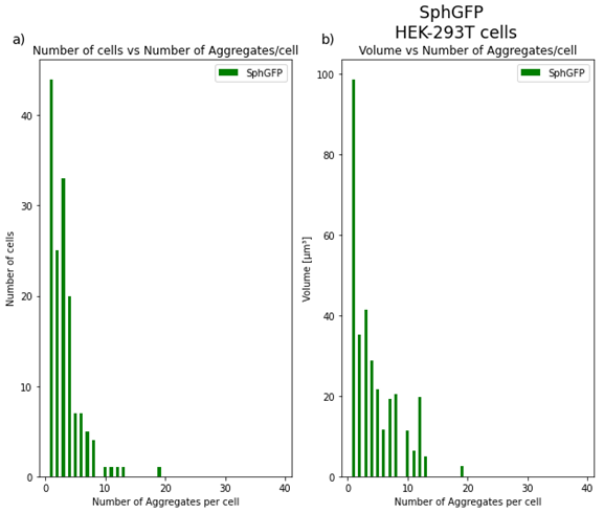

Figure 4. Relation of number of cells and volume of aggregates with number of aggregates per cell. The average volume per N in confocal microscopy. a) Bar plot of number of cells vs the number of aggregates in the Sph1-GFP aggregation model using confocal microscopy. b) Bar plot of average volume of the aggregates in each number of aggregates per cell in Sph1-GFP aggregation model using confocal microscopy.

the variables in analysis (Table 1), these results can be discuss using several views of 3D projections to access the location of the aggregate and shape of it across all axes (Figure and Figure 3). The volume of confocal microscopy (32,36 ± 62,59 µm3) contrast with the result from STED microscopy (6,44 ± 27,39 µm3), this result has a difference of around one order of difference. This difference is kept in the same order in number of aggregates per cell in which the number of aggregates detected are higher in STED microscopy (3 ± 2 – confocal – and 8 ± 13 – STED) and the volume of aggregates per cell (50,75 ± 55,77 µm3 – confocal – and 24,57 ± 37,60 µm3 - STED).

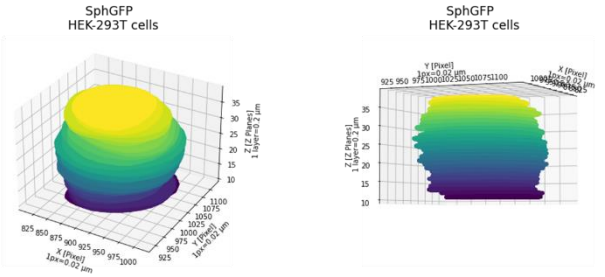

Figure 5. Several views of the 3D projection from STED microscopy in the Sph1-GFP aggregation model.

After concluding the difference in terms of volume and number of aggregates in each microscopy, the distribution of this values was analyzed in function to the number of aggregates per cell (Figure and Figure 6). In confocal microscopy, both relations look a hyperbole with higher number of cell where it was found lower number of aggregates (Figure a) and the volume of those aggregates are higher in smaller number of aggregates per cell (Figure b).

As it was expected, the results from STED microscopy were similar in terms of shape of the aggregate (Figure). Regarding the STED microscopy, the relation is kept in both bar plots – large number of

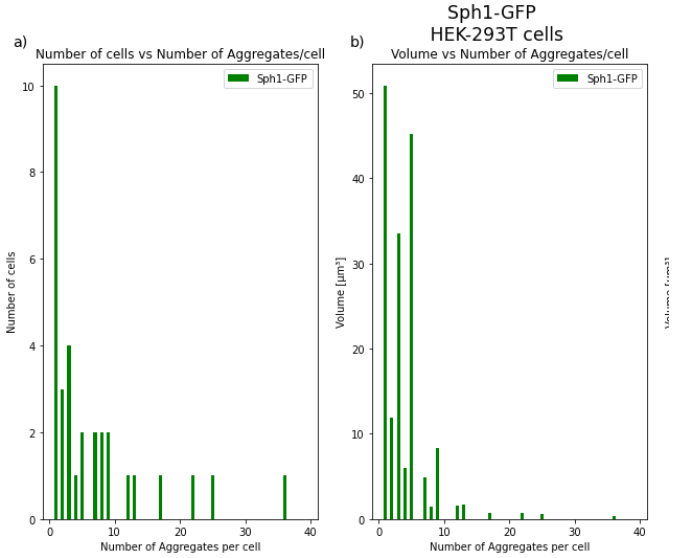

Figure 6. Relation of number of cells and volume of aggregates with number of aggregates per cell. The average volume per N in STED microscopy. a) Bar plot of number of cells vs the number of aggregates in the Sph1-GFP aggregation model using STED microscopy. b) Bar plot of average volume of the aggregates in each number of aggregates per cell in Sph1-GFP aggregation model using STED microscopy.

cells with small number of aggregates and the volume of those aggregates are higher than when there are more than 5 aggregates. The results look a hyperbole although the range of number of aggregates per cell differ from confocal microscopy

In the other model SynTWT+Sph1 aggregation model, as it was expected that smaller aggregates in terms of volume but many aggregates per cell (Table 2). This hypothesis can be discussed using several views of 3D projections (Figure and Figure 9) to access the location and therefore the possible interaction between the protein in question.

Table 2. Values of average and standard deviation regarding the volume of aggregates, number of aggregates per cell and the average volume of aggregates per cell in SynTWT+Sph1 aggregation model.

Type of Microscopy	Average Volume of aggregates [µm^3]	Average Number of aggregates per cell [aggregates]	Average Volume of aggregates per cell [µm^3]
Confocal SynTWT	2,37 ± 3,61	14 ± 13	2,12 ± 1,83
STED SynTWT	0,9 ± 1,51	18 ± 11	0,88 ± 0,6
Confocal Sph1	2,77 ± 4,21	11 ± 10	3,17 ± 2,29
STED Sph1	1,70 ± 2,70	14 ± 8	1,81 ± 1,30

The volume of aggregates using confocal microscopy show little difference in comparison with the result from STED microscopy. This difference is kept in the same order in number of aggregates per cell in both signals (SynTWT: 14 ± 13– confocal – and– 18 ± 11 - STED; Sph1: 11 ± 10 – confocal – and - 14 ± 8 - STED) and the volume of aggregates per cell (SynTWT: 2,12 ± 1,83– confocal – and– 0,88 ± 0,6 - STED; Sph1: 3,17 ± 2,29 – confocal – and - 1,81 ± 1,30 - STED).

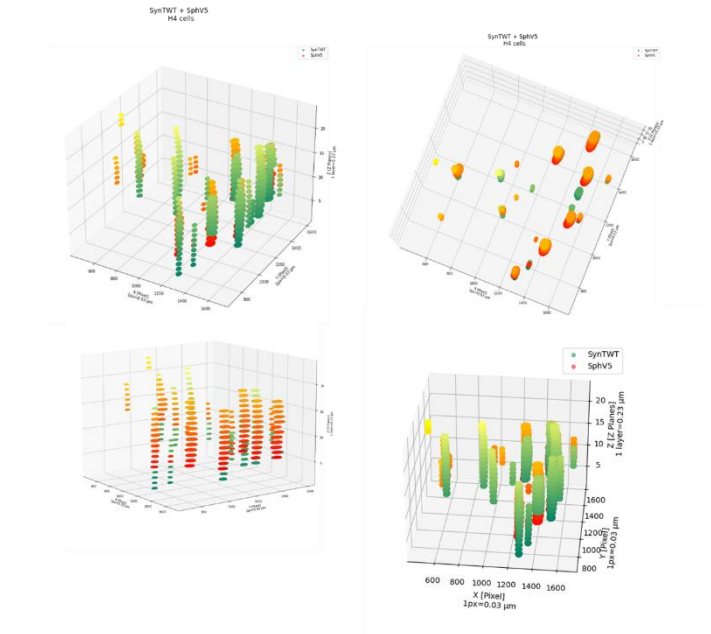

Figure 7. Several views of the 3D projection from confocal microscopy in the SynTWT+Sph1 aggregation model. These views are the analysis of the segmented areas and MIP image from confocal microscopy and SynTWT+Sph1 aggregation model.

After analysing the difference in terms of volume and number of aggregates in each microscopy, the distribution of number of cells and volume was analyzed in function to the number of aggregates per cell (Figure 8 and Figure 10).

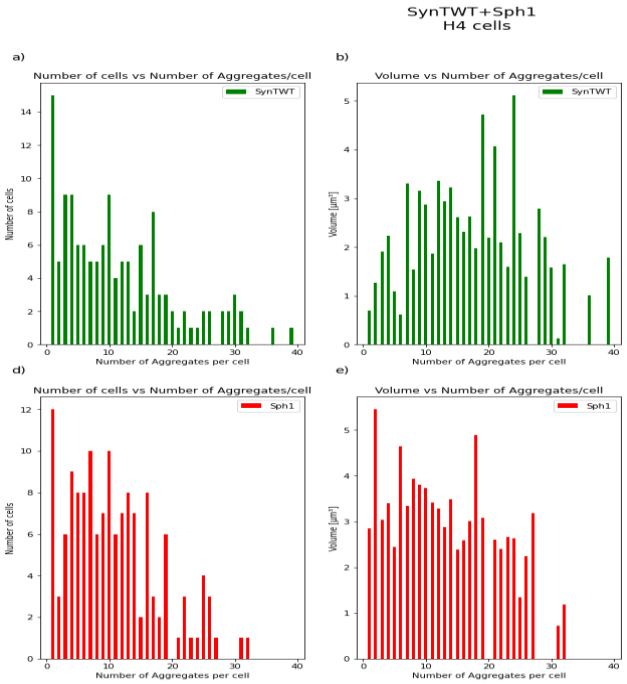

Figure 8. Relation of number of cells and volume of aggregates with number of aggregates per cell. The average volume per N in confocal microscopy for each channel of interest (SynTWT-top and Sph1-bottom). a) Bar plot of number of cells vs the number of aggregates regarding the SynTWT channel in the SynTWT+Sph1 aggregation model using confocal microscopy. b) Bar plot of average volume of the aggregates in each number of aggregates per cell regarding SynTWT channel in SynTWT+Sph1 aggregation model using confocal microscopy. d) Bar plot of number of cells vs the number of aggregates regarding the Sph1 channel in the SynTWT+Sph1 aggregation model using confocal microscopy. e) Bar plot of average volume of the aggregates in each number of aggregates per cell regarding Sph1 channel in SynTWT+Sph1 aggregation model using confocal microscopy.

The distribution of the number of cells in function of the number of aggregates per cell looks a hyperbole in both channels, although there are some disruptive values in the Sph1 channel (Figure d). Comparing in terms of volume of aggregates in function of the number of aggregates per cell, in SynTWT signal looks a Gaussian distribution in contrast with the Sph1 channel where looks constant. It indicates that in SynTWT, it is possible that the number of aggregates in the cell affects the volume of those aggregates in contrast with the Sph1 channel where looks independent of the number of aggregates per cell.

The same protocol was used to locate and evaluate the spatial localization of the different aggregates (Figure 9). It is clear the small difference regarding the shape of the aggregate with more detail although less compact the aggregates in a more random distribution in space.

The distribution of the number of cells in function of the number of aggregates per cell cannot be taken due to small number of images analysed, this reason can be applied to both channels (Figure 10a, d). Comparing in terms of volume of aggregates in function of the number of aggregates per cell, in SynTWT and Sph1 signal looks again a Gaussian distribution (Figure

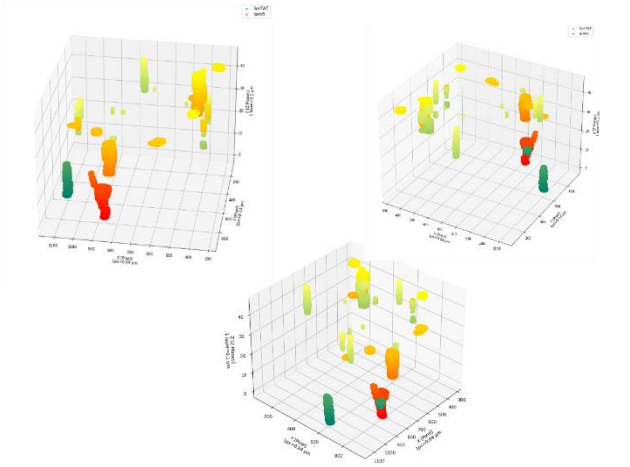

Figure 9. Several views of the 3D projection from STED microscopy in the SynTWT+SphV5 aggregation model. These views are the analysis of the segmented areas and MIP image from confocal microscopy and SynTWT+SphV5 aggregation model.

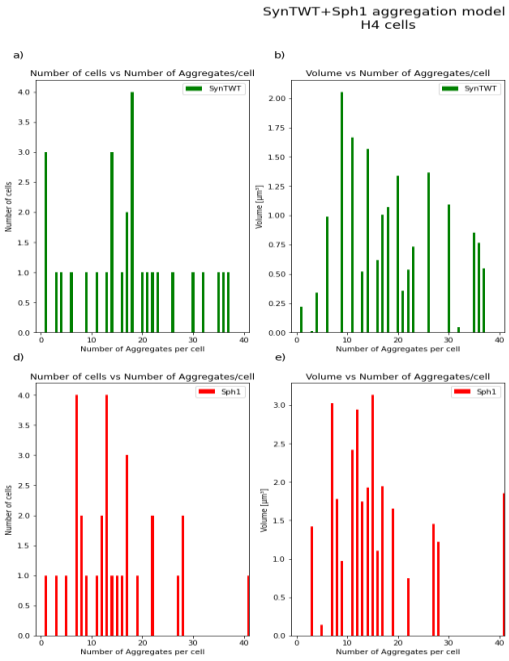

Figure 10. Relationship between number of cells and volume of aggregates with number of aggregates per cell. The average volume per N in STED microscopy for each channel of interest (SynTWT-top and Sph1-bottom). a) Bar plot of number of cells vs the number of aggregates regarding the SynTWT channel in the SynTWT+Sph1 aggregation model using STED microscopy. b) Bar plot of average volume of the aggregates in each number of aggregates per cell regarding SynTWT channel in SynTWT+Sph1 aggregation model using STED microscopy.d) Bar plot of number of cells vs the number of aggregates regarding the Sph1 channel in the SynTWT+Sph1 aggregation model using STED microscopy. e) Bar plot of average volume of the aggregates in each number of aggregates per cell regarding Sph1 channel in SynTWT+Sph1 aggregation model using STED microscopy.

10b, e)

To study the interaction between these two proteins, we used an object-based colocalization based on the colocalization of Sph1 in relation of SynTWT (Table 3). It is observed that there are some colocalization between them although the mean colocalization is lower, the maximum colocalization can reach values where in some slices the intersection between them is high.

Table 3. Average and standard deviation of mean colocalization and maximum colocalization between the Sph1 and SynTWT signal.

Type of Microscopy	Mean of Colocalization	Maximum Colocalization
Confocal	13,61 ± 12,71 %	53,61 ± 37,89 %
STED	15,46 ± 12,62 %	69.42 ± 36.35 %

The values given by the colocalization analysis helps in the hypothesis of interaction between the proteins as can be seen as well in the 3D projections.

Discussion

The aggregation of αSyn is a central hallmark of several neurodegenerative diseases such as PD, however, the study of the biology and functions behind it remain poorly understood. Fluorescence microscopy has been a resourceful tool used in experiments in both cell and animal studies. Therefore, using fluorescence microscopy to analyse some of the aggregation model has been the major source of information.

Most of the images so far have been analysed in Maximum Intensity Projection which led to results and characterization of 2D images and carrying the problem of the localization in space. Thus, focusing on understanding how these aggregates are located in space is the next step in both the field of microscopy and biology. On one hand, the progress to find better techniques of analysis and setups to have a better resolution in all possible axes has been the major focus of microscopy. On the other hand, the accuracy of images and data help the biology to get a better understanding of some neurodegenerative diseases. Thus, both fields of study need to be in parallel and complement each other for best results leading to progress. Analysing these images can use several protocols (Meijering et al., 2004; Puchkov, 2021; Rizk et al., 2014), the most important factor is the segmentation of the regions of interest. Deconvolution of the images and the creation of PSF to deconvolute can be the most accurate way to analyse (Rizk et al., 2014) although it is very bias to the interpretation of the user. Removing some noise using a given signal to noise ratio can improve the results as well. The protocol used in this study is very similar with (Rizk et al., 2014), although less features of the aggregate and less pre-processing of the image was done like the ones explained above. Therefore, this study can be used as a baseline to improve with more steps though the protocol to improve the accuracy of the protocols

One of the goals of the work was to create a volumed analysis of some aggregate models, this goal was achieved using a deep learning algorithm (Stardist (Schmidt et al., 2018; Weigert et al., 2020)) to segment in several aggregates and the relationship between those predicted slices. This method can be used in convex-shape polygon aggregates in order to get a volume of aggregate instead of area.

Another goal of the work was to compare different types of microscopy techniques to ensure what microscopy could be more suitable for the aggregation model in question. This goal was achieved using several techniques in different ranges of resolutions.

The hypothesis of finding the most suitable technique depending on the aggregation model in this study marks an important step to the way of analysing the spatial location of protein aggregation in the cell and the interaction of several proteins combining a more cost-efficient way of imaging the protein aggregation model. Therefore, comparing the results gathered and the time taken to record the data in both models, probably using STED in the Sph1-GFP aggregation model does not make it profitable to use due to the time spent in the technique. Although, the SynTWT+Sph1 aggregation model can be advantageous due to the number of aggregates and the size of them.

Sph1-GFP aggregation model

Sph1 was studied in terms of formation of inclusions (Büttner et al., 2010), colocalization with several proteins (Chung et al., 2001) and its role in the PD (Krüger, 2004) although the analysis of the fluorescence images has been done by the number of aggregates or the area of those aggregates or even colocalization to other proteins by MIP or just a slice of the entire image. Therefore, the use of the real appearance of the protein can give better clues in the previous described topics.

Analysing the relation to the number of cells in function of the number of aggregates per cell and the average volume in function of the number of aggregates per cell, some hypothesis can be raised. Comparing the number of cells in function of the number of aggregates per cell in each microscopy technique (Figure 4a, Figure 6a), the shape of the graphs looks similar, but one difference needs to be taken in consideration. The low number of cells in STED microscopy probably can explain this difference in values. This reason can be transported to the average volume in function of the number of aggregates per cell where a small number of pictures taken can be a problem. When the number of aggregates is low, the average volume of those aggregates is big, achieving almost 100 μm^3 in confocal microscopy and 50 μm^3 in STED microscopy.

To understand the weight of each aggregate in the analysis and results, two different types of averaging were performed. (Volume of aggregates and volume of aggregates per cell). Between the two variables, the difference is kept at the same level unless one difference can be taken. When all the aggregates have the same weight in the average, the result is lower which indicates that there are a lot of aggregates with a very small volume, but it is not dispersive through all cells. This might be due to the majority having large aggregates. The number of aggregates per cell corroborates the difference found between microscopy techniques, using STED, there are almost 3 times more aggregates per cell with a bigger range of values in contrast when compared in confocal microscopy

To access the position of the aggregates together with its volume, several statistical metrics was evaluated (volume of aggregates, number of aggregates per cell and volume of aggregates per cell). This metrics were applied in both microscopies as well as in both aggregation models.

This lack of similarity between these two types of microscopes can have several reasons. One reason can be the Z resolution. It used a 2D STED which then, some light can be transferred from different slices, this problem can happen in Confocal Microscopy, in other words, the PSF for each type of microscopy would be different. Another reason that can explain by the images used in the training. The model was trained with confocal microscopy images and one possibility of overcoming the issues would be to use images from STED to train the model. Another reason can be the difference of number of images, increasing the number of cells analysed in STED microscopy can be a solution or a way to test this hypothesis. Finally, using the 3D STED setup can be a solution as well in order to increase the resolution in the Z axis.

SynTWT+Sph1 aggregation model

Both proteins were studied in several ways using several techniques in most of them analyse microscopy images in terms of areas (Nath et al., 2011) or number (Lázaro et al., 2014) reaching very small size and high number aggregates but reaching the values in terms of volume gives a more accurate result to the real aspect of the aggregate.

According to the previous 3D projection of this aggregation model in confocal and STED microscopy, it looks that the size and shape are similar in the essence with difference in the shape and space location. Although when we statistically compare the results (Table 2), the average result is quite similar between the two. In our study, we expected to have differences between the two types of microscopy techniques in terms of average aggregate volumes due to the small sizes, which could be facilitating the differentiation between the Confocal and STED microscopy in terms of principles but that did not happen.

In the SynTWT channel, the shape of the graph almost looks like a Gaussian distribution where the bigger aggregates can be found between 10 and 30 aggregates per cell. In contrast, the Sph1 channel, the shape of the graph looks more constant in function of the number of aggregates per cell. Therefore, we can assume that the volume of the aggregate is influenced by the number of aggregates in the cell in the SynTWT channel while it is not influenced in the Sph1 channel.

Comparing the different values for volume of aggregates and volume of aggregates per cell between channels and types of microscopies can lead to several hypotheses. Considering the SynTWT and Sph1 of Confocal Microscopy, the size of Sph1 aggregates is higher than SynTWT in both ways of calculating the average volume; that same relation is also applied in STED microscopy. The standard deviation of Sph1 aggregates is higher than SynTWT aggregates which can indicate a bigger range of values in terms of volume which can corroborate the idea of no interference of the number of aggregates per cell in contrast with the SynTWT aggregates (Luk et al., 2009).

Although several proteins have been linked with aggregation of αSyn (Büttner et al., 2010; Casadei et al., 2014; Chung et al., 2001; Liani et al., 2004; Lücking & Brice, 2000; Ribeiro et al., 2002; Swinnen et al., 2011), the hypothesis of interaction and therefore colocalization has been tested using several techniques (Luk et al., 2009). The study described that there is possible the interaction between them due to the fact of there are some colocalization. If we compare the results given by an object-based colocalization, the interaction does not seem very high. Checking several positions in

the 3D projections of those proteins, it seems that interaction is different in terms of the Z axis. In other words, the Sph1 protein looks translated in Z compared with SynTWT protein. From previous studies in which it was used electron microscopy (Luk et al., 2009), it is described the position of the aggregates closer and starting closer to the nucleus. That statement cannot be verified since the segmentation of the nucleus was not done. Using 3D STED could improve that differentiation in the axis to improve the capability of getting more accurate volumes of the aggregates.

These results can lead us to doubt about the real interaction between the aggregates and using different types of colocalization can be advantageous to classify that interaction.

Expansion Microscopy

Expansion Microscopy can lead us to several breakthroughs in terms of microscopy but still a lot to work on in terms of stability of the sample and viability of the protocols. The use of simple microscopes takes this technique to a very high ratio between results and feasibility.

The stability of the sample was the most difficult aspect to deal with. The expansion factor achieved during the experiments was 5.15 which is below present in (Truckenbrodt et al., 2018, 2019). Although, this technique can be used to overcome the diffraction limit, combining with confocal or STED can even more improve the resolution than it was achieved before (Truckenbrodt et al., 2018; Zwettler et al., 2020). In Figure 15c, the background of the images is much larger than another type of microscopy presented in this work due to the use of a gel instead of glass lamine with a more dispersive light in the gel. Therefore, this microscopy will need several steps before taking the same type of analysis. The filtering of the microscope will need to be very accurate because of the extensive time of exposure and the possibility of having signals in channels that we didn't desire. In order to remove some signal that can pass through to other channels, adaptative filters can be used (Peli & Lim, 1981).

To sum up, this study provided a method to evaluate the volume of the aggregates from two aggregate models associated with PD and the comparison between different microscopy in order to understand what the advantages are of using each technique. We also used some computational analysis which removed some biases that happen in the manual analysis by the researchers performing the studies. This could be used for a better time and cost efficiency in the future studies using the same models of aggregation and testing some possible therapeutic approaches.

Acknowledgments

This document was written and made available as an institutional academic requirement and as a part of the evaluation of the MSc thesis in Bioengineering and Nanosystems of the author at Instituto Superior Técnico. The work described herein was performed at the University Medical Center Göttingen in Göttingen, Germany.

References

Biontex. (n.d.). *Transfection Methods*. Retrieved June 12, 2021, from https://www.biontex.com/en/transfection/

Bossy-Wetzel, E., Schwarzenbacher, R., & Lipton, S. A. (2004). Molecular pathways to neurodegeneration. *Nature Medicine*, *10*(7), S2–S9. https://doi.org/10.1038/nm1067

Burré, J., Sharma, M., Tsetsenis, T., Buchman, V., Etherton, M., & Südhof, T. C. (2010). *α-Synuclein Promotes SNARE-Complex Assembly in vivo and in vitro* (Vol. 329, Issue 5999).

Büttner, S., Delay, C., Franssens, V., Bammens, T., Ruli, D., Zaunschirm, S., de Oliveira, R. M., Outeiro, T. F., Madeo, F., Buée, L., Galas, M. C., & Winderickx, J. (2010). Synphilin-1 enhances a-synuclein aggregation in yeast and contributes to cellular stress and cell death in a sir2-dependent manner. *PLoS ONE*, *5*(10). https://doi.org/10.1371/journal.pone.0013700

Casadei, N., Pö Hler, A.-M., Tomá S-Zapico, C., Torres-Peraza, J. S., Schwedhelm, I., Witz, A., Zamolo, I., De Heer, R., Spruijt, B., Noldus, L. P. J. J., Klucken, J., Lucas, J. J., Kahle, P. J., Krü Ger, R., Riess, O., & Nuber, S. (2014). Overexpression of synphilin-1 promotes clearance of soluble and misfolded alpha-synuclein without restoring the motor phenotype in aged A30P transgenic mice. *Human Molecular Genetics*, *23*(3), 767–781. https://doi.org/10.1093/hmg/ddt467

Chozinski, T. J., Halpern, A. R., Okawa, H., Kim, H. J., Tremel, G. J., Wong, R. O. L., & Vaughan, J. C. (2016). Expansion Microscopy with Conventional Antibodies and Fluorescent Proteins. *Nature Methods*, *13*(6), 485. https://doi.org/10.1038/NMETH.3833

Chung, K. K. K., Zhang, Y., Lim, K. L., Tanaka, Y., Huang, H., Gao, J., Ross, C. A., Dawson, V. L., & Dawson, T. M. (2001). Parkin ubiquitinates the α-synuclein–interacting protein, synphilin-1: implications for Lewy-body formation in Parkinson disease. *Nature Medicine*, *7*(10), 1144–1150. https://doi.org/10.1038/nm1001-1144

Conway, K. A., Rochet, J. C., Ding, T. T., Harper, J. D., Williamson, R. E., & Lansbury, P. T. (2000). Accelerated Oligomerization by Parkinson's Disease Linked α-Synuclein Mutants. *Annals of the New York Academy of Sciences*, *920*(1), 42–45. https://doi.org/10.1111/J.1749-6632.2000.TB06903.X

Cuervo, A. M., Stafanis, L., Fredenburg, R., Lansbury, P. T., & Sulzer, D. (2004). Impaired degradation of mutant α-synuclein by chaperone-mediated autophagy. *Science*, *305*(5688), 1292–1295. https://doi.org/10.1126/SCIENCE.1101738/SUPPL_FILE/CUERVO.SOM.PDF

Gitler, A. D., Dhillon, P., & Shorter, J. (2017). Neurodegenerative disease: Models, mechanisms, and a new hope. *DMM Disease Models and Mechanisms*, *10*(5), 499–502. https://doi.org/10.1242/DMM.030205

Goedert, M. (2001). Alpha-synuclein and neurodegenerative diseases. *Nature Reviews Neuroscience*, *2*(7), 492–501. https://doi.org/10.1038/35081564

Gonçalves, S., & Outeiro, T. F. (2013). Assessing the subcellular dynamics of alpha-synuclein using photoactivation microscopy. *Molecular Neurobiology*, *47*(3), 1081–1092. https://doi.org/10.1007/s12035-013-8406-x

Greten-Harrison, B., Polydoro, M., Morimoto-Tomita, M., Diao, L., Williams, A. M., Nie, E. H., Makani, S., Tian, N., Castillo, P. E., Buchman, V. L., & Chandra, S. S. (2010). αβγ-Synuclein triple knockout mice revealage-dependent neuronal dysfunction. *Proceedings of the National Academy of Sciences of the United States of America*, *107*(45), 19573–19578. https://doi.org/10.1073/pnas.1005005107

Huang, Y., Cheung, L., Rowe, D., & Halliday, G. (2004). Genetic contributions to Parkinson's disease. *Brain Research Reviews*, *46*(1), 44–70. https://doi.org/10.1016/J.BRAINRESREV.2004.04.007

Krüger, R. (2004). The role of synphilin-1 in synaptic function and protein degradation. In *Cell and Tissue Research* (Vol. 318, Issue 1, pp. 195–199). https://doi.org/10.1007/s00441-004-0953-z

Lázaro, D. F., Rodrigues, E. F., Langohr, R., Shahpasandzadeh, H., Ribeiro, T., Guerreiro, P., Gerhardt, E., Kröhnert, K., Klucken, J., Pereira, M. D., Popova, B., Kruse, N., Mollenhauer, B., Rizzoli, S. O., Braus, G. H., Danzer, K. M., & Outeiro, T. F. (2014). Systematic Comparison of the Effects of Alpha-synuclein Mutations on Its Oligomerization and Aggregation. *PLoS*

Genetics, *10*(11). https://doi.org/10.1371/journal.pgen.1004741

Li, J., Uversky, V. N., & Fink, A. L. (2001). Effect of Familial Parkinson's Disease Point Mutations A30P and A53T on the Structural Properties, Aggregation, and Fibrillation of Human α-Synuclein†. *Biochemistry*, *40*(38), 11604–11613. https://doi.org/10.1021/BI010616G

Liani, E., Eyal, A., Avraham, E., Shemer, R., Szargel, R., Berg, D., Bornemann, A., Riess, O., Ross, C. A., Rott, R., & Engelender, S. (2004). Ubiquitylation of synphilin-1 and α-synuclein by SIAH and its presence in cellular inclusions and Lewy bodies imply a role in Parkinson's disease. *Proceedings of the National Academy of Sciences of the United States of America*, *101*(15), 5500–5505. https://doi.org/10.1073/pnas.0401081101

Lücking, C. B., & Brice, A. (2000). Alpha-synuclein and Parkinson's disease. *Cellular and Molecular Life Sciences CMLS 2000 57:13*, *57*(13), 1894–1908. https://doi.org/10.1007/PL00000671

Luk, K. C., Song, C., O'Brien, P., Stieber, A., Branch, J. R., Brunden, K. R., Trojanowski, J. Q., & Lee, V. M. Y. (2009). Exogenous α-synuclein fibrils seed the formation of Lewy body-like intracellular inclusions in cultured cells. *Proceedings of the National Academy of Sciences of the United States of America*, *106*(47), 20051–20056. https://doi.org/10.1073/pnas.0908005106

Marvian, A. T., Koss, D. J., Aliakbari, F., Morshedi, D., & Outeiro, T. F. (2019). In vitro models of synucleinopathies: informing on molecular mechanisms and protective strategies. *Journal of Neurochemistry*, *150*(5), 535–565. https://doi.org/10.1111/jnc.14707

McLean, P. J., Kawamata, H., Ribich, S., & Hyman, B. T. (2000). Membrane Association and Protein Conformation of α-Synuclein in Intact Neurons: EFFECT OF PARKINSON'S DISEASE-LINKED MUTATIONS *. *Journal of Biological Chemistry*, *275*(12), 8812–8816. https://doi.org/10.1074/JBC.275.12.8812

Meijering, E., Jacob, M., Sarria, J.-C. C. F., Steiner, P., Hirling, H., & Unser, M. (2004). Design and Validation of a Tool for Neurite Tracing and Analysis in Fluorescence Microscopy Images. *Cytometry Part A*, *58*(2), 167–176. https://doi.org/10.1002/cyto.a.20022

Nath, S., Goodwin, J., Engelborghs, Y., & Pountney, D. L. (2011). Raised calcium promotes α-synuclein aggregate formation. *Molecular and Cellular Neuroscience*, *46*(2), 516–526. https://doi.org/10.1016/J.MCN.2010.12.004

Outeiro, T. F., & Mestre, T. A. (2019). Synuclein Meeting 2019: where we are and where we need to go. *Journal of Neurochemistry*, *150*(5), 462–466. https://doi.org/10.1111/jnc.14825

Pawley, J. (2006). *Confocal Handbook.Pdf* (p. 4).

Peli, T., & Lim, J. (1981). Adaptive filtering for image enhancement. *ICASSP '81. IEEE International Conference on Acoustics, Speech, and Signal Processing*, *6*, 1117–1120. https://doi.org/10.1109/ICASSP.1981.1171130

Puchkov, E. O. (2021). Computerized fluorescence microscopy of microbial cells. In *World Journal of Microbiology and Biotechnology* (Vol. 37, Issue 11, p. 189). https://doi.org/10.1007/s11274-021-03159-3

Ribeiro, C. S., Carneiro, K., Ross, C. A., Menezes, J. R. L., & Engelender, S. (2002). Synphilin-1 is developmentally localized to synaptic terminals, and its association with synaptic vesicles is modulated by α-synuclein. *Journal of Biological Chemistry*, *277*(26), 23927–23933. https://doi.org/10.1074/JBC.M201115200

Rizk, A., Paul, G., Incardona, P., Bugarski, M., Mansouri, M., Niemann, A., Ziegler, U., Berger, P., & Sbalzarini, I. F. (2014). Segmentation and quantification of subcellular structures in fluorescence microscopy images using Squassh. *Nature Protocols*, *9*(3), 586–596. https://doi.org/10.1038/nprot.2014.037

Schmidt, U., Weigert, M., Broaddus, C., & Myers, G. (2018). Cell detection with star-convex polygons. *Lecture Notes in Computer Science (Including Subseries Lecture Notes in Artificial Intelligence and Lecture Notes in Bioinformatics)*, *11071 LNCS*, 265–273. https://doi.org/10.1007/978-3-030-00934-2_30

Schulz-Schaeffer, W. J. (2015). Is Cell Death Primary or Secondary in the Pathophysiology of Idiopathic Parkinson's Disease? *Biomolecules*, *5*(3), 1467–1479. https://doi.org/10.3390/BIOM5031467

Shirakashi, Y., Kawamoto, Y., Tomimoto, H., Takahashi, R., & Ihara, M. (2006). α-Synuclein is colocalized with 14-3-3 and synphilin-1 in A53T transgenic mice. *Acta Neuropathologica*, *112*(6), 681–689. https://doi.org/10.1007/S00401-006-0132-2

Swinnen, E., Büttner, S., Outeiro, T. F., Galas, M. C., Madeo, F., Winderickx, J., & Franssens, V. (2011). Aggresome formation and segregation of inclusions influence toxicity of α-synuclein and synphilin-1 in yeast. *Biochemical Society Transactions*, *39*(5), 1476–1481. https://doi.org/10.1042/BST0391476

Tanaka, M., Kim, Y. M., Lee, G., Junn, E., Iwatsubo, T., & Mouradian, M. M. (2004). Aggresomes Formed by α-Synuclein and Synphilin-1 Are Cytoprotective. *Journal of Biological Chemistry*, *279*(6), 4625–4631. https://doi.org/10.1074/JBC.M310994200

Truckenbrodt, S., Maidorn, M., Crzan, D., Wildhagen, H., Kabatas, S., & Rizzoli, S. O. (2018). X10 expansion microscopy enables 25-nm resolution on conventional microscopes. *EMBO Reports*, *19*(9). https://doi.org/10.15252/embr.201845836

Truckenbrodt, S., Sommer, C., Rizzoli, S. O., & Danzl, J. G. (2019). A practical guide to optimization in X10 expansion microscopy. *Nature Protocols*, *14*(3), 832–863. https://doi.org/10.1038/s41596-018-0117-3

Valente, E. M., Arena, G., Torosantucci, L., & Gelmetti, V. (2012). Molecular pathways in sporadic PD. *Parkinsonism & Related Disorders*, *18*(SUPPL. 1), S71–S73. https://doi.org/10.1016/S1353-8020(11)70023-2

van Dort, J. (2018). *Aberration correction in STED microscopy*. *October*, 1–74. https://ediss.uni-goettingen.de/bitstream/handle/21.11130/00-1735-0000-0005-12B4-B/Dissertation_JorisvanDort.pdf?sequence=1

Vidyadhara, D. J., Lee, J. E., & Chandra, S. S. (2019). Role of the endolysosomal system in Parkinson's disease. *Journal of Neurochemistry*, *150*(5), 487–506. https://doi.org/10.1111/jnc.14820

Wakabayashi, K., Engelender, S., Tanaka, Y., Yoshimoto, M., Mori, F., Tsuji, S., Ross, C. A., & Takahashi, H. (2001). Immunocytochemical localization of synphilin-1, an α-synuclein-associated protein, in neurodegenerative disorders. *Acta Neuropathologica 2001 103:3*, *103*(3), 209–214. https://doi.org/10.1007/S004010100451

Wegner, W., Ilgen, P., Gregor, C., Van Dort, J., Mott, A. C., Steffens, H., & Willig, K. I. (2017). In vivo mouse and live cell STED microscopy of neuronal actin plasticity using far-red emitting fluorescent proteins. *Scientific Reports*, *7*(1). https://doi.org/10.1038/s41598-017-11827-4

Weigert, M., Schmidt, U., Haase, R., Sugawara, K., & Myers, G. (2020). Star-convex polyhedra for 3D object detection and segmentation in microscopy. *Proceedings - 2020 IEEE Winter Conference on Applications of Computer Vision, WACV 2020*, 3655–3662. https://doi.org/10.1109/WACV45572.2020.9093435

Willig, K. I., Steffens, H., Gregor, C., Herholt, A., Rossner, M. J., & Hell, S. W. (2014). Nanoscopy of filamentous actin in cortical dendrites of a living mouse. *Biophysical Journal*, *106*(1). https://doi.org/10.1016/J.BPJ.2013.11.1119

Xie, Y.-Y., Zhou, C.-J., Zhou, Z.-R., Hong, J., Che, M.-X., Fu, Q.-S., Song, A.-X., Lin, D.-H., & Hu, H.-Y. (2010). Interaction with synphilin-1 promotes inclusion formation of α-synuclein: mechanistic insights and pathological implication. *The FASEB Journal*, *24*(1), 196–205. https://doi.org/10.1096/fj.09-133082

Zwettler, F. U., Reinhard, S., Gambarotto, D., Bell, T. D. M., Hamel, V., Guichard, P., & Sauer, M. (2020). Molecular resolution imaging by post-labeling expansion single-molecule localization microscopy (Ex-SMLM). *Nature Communications*, *11*(1). https://doi.org/10.1038/s41467-020-17086-8